Numerical Simulation of Viscous Fingering Phenomenon in Immiscible Displacement of Two Fluids in Porous Media Using Lattice Boltzmann Method

Bo DONG [1, 2], Yuying YAN [1,*], Weizhong LI [2]

* Corresponding author: Tel.: ++44 (0)115 951 3169; Fax: ++44 (0)115 951 3159; Email: yuying.yan@nottingham.ac.uk
1: School of the Built Environment, University of Nottingham, UK
2: School of Energy and Power Engineering, Dalian University of Technology, Dalian, China

Abstract In the present study, viscous fingering phenomenon, which occurs when a less viscous fluid (e.g. supercritical carbon dioxide) is injected into simplified porous media to displace a more viscous fluid (e.g. crude oil), is investigated by a mesoscopic approach-the lattice Boltzmann method (LBM). Due to its convenience in dealing with complex fluids of different viscosities, the pseudo-potential model is employed to study the effects of the capillary number, Bond number and viscosity ratio between the displaced fluids and displacing fluid; as such effects reflect the competition of viscous force and surface tension and gravity forces during viscous fingering. The numerical procedure is validated against a series of droplet tests, in which surface tension can be determined. By changing the injecting velocity of the displacing fluid and gravitational acceleration, the displacement processes under conditions of different capillary number and Bond number are investigated. The finger pattern is presented in this paper. The effects of capillary number, Bond number and viscosity ratio are discussed in detail. The ability and suitability of the lattice Boltzmann method for simulating multi-component fluids displacement in porous media are proved in our work.

Keywords: Porous media, Immiscible fluids, Viscous fingering phenomenon, Lattice Boltzmann method

1. Introduction

Fluid flow in porous media is of great interest in many industrial applications such as oil recovery, geological sequestration of carbon dioxide, imbibition and underground pollutant remedy application. In the oil industry, gas injection is the most commonly used approach to enhance oil recovery. However, when the viscosity of residual oil is higher than that of the injected gas, the displacement may become unstable and result in the onset of viscous fingering, which is recognised as a serious problem because its early appearance can lead to poor recovery efficient.

In recent years, the LBM has achieved rapid development and served as an alternative and powerful tool for numerical modelling of the fluid dynamics. Due to its kinetic nature and easy implementation in complex geometry by using bounce-back boundary condition, it has been widely used to study transport phenomena in porous media (van Kats and Egberts 1999; Grosfils et al. 2004; Yiotis et al. 2007; Huang et al. 2008). As for immiscible fluid displacement process in porous media, the behaviour of the interface front yields complicated patterns which reflect intricate interplay between viscous force, capillary force and gravity. In their research, the effects of capillary number or viscosity ratio on the immiscible fluid behaviour in porous media have been investigated in detail; however, most of them ignored the effect of gravity on viscous fingering phenomenon. Even if the gravity was mentioned, but no attention has been paid on this factor.

In this paper, lattice Boltzmann method is employed to study the effects of capillary number, Bond number, and viscosity ratio between the displaced fluid and the displacing fluid on the viscous fingering phenomenon of immiscible fluid displacement process in simplified porous media with consideration of gravity.

2. Theory and Model

In the LBM, the fluid is modelled as a

collection of discrete sets of particles colliding at a regular lattice and moving from site to site along the edges of the lattice while the mass and momentum of the fluid are conserved, respectively. Several models are available to simulate multiphase or multi-component fluid flow behaviour. The first one, introduced by Gunstensen and Rothman for immiscible fluids (Gunstensen and Rothman 1991), is known as chromodynamics model, in which the fluid is colored either red or blue and a special collision rule is introduced to account for the properties of immiscible fluids. Shan et al. developed a new model, known as pseudo-potential model, by introducing pseudo-potential function to achieve phase separation automatically (Shan and Chen 1993; Shan and Doolen 1995). Swift et al. proposed the free energy model that uses a non ideal pressure tensor and external chemical potential instead of additional collision operator, so that one can obtain an isothermal model of phase separation which correctly describes bulk and interfacial dynamics at low temperatures (Swift and Yeomans 1995; Swift et al. 1996). The other models include the one proposed by Luo (1998, 2000) by discretizing Enskog equation in both phase space and time space, and the one developed by He et al. (He, Chen and Zhang 1999) which introduces a index function to indicate the evolution of the interface.

All of the above models have their own advantages and disadvantages. How to choose a suitable model depends on the research focus and the application of interest. In the present study, pseudo-potential D2Q9 model is chosen due to its ease to deal with fluids with different viscosities and its convenience to handle complex interaction.

In pseudo-potential D2Q9 model, lattice BGK model is extended to multi-component by using different sets of particle distribution functions (PDFs) for each fluid component. The evolution of PDFs is based on Eq. (1), given as

$$f_\alpha^\sigma\left(\mathbf{x}+\mathbf{e}_\alpha\delta_t, t+\delta_t\right) = f_\alpha^\sigma\left(\mathbf{x},t\right) - \frac{1}{\tau^\sigma}\left[f_\alpha^\sigma\left(\mathbf{x},t\right) - f_\alpha^{\sigma(eq)}\left(\mathbf{x},t\right)\right] \quad (1)$$

where $f_\alpha^\sigma(\mathbf{x},t)$ is the particle distribution function of the σth fluid component at position $\mathbf{x}$ at time t; $f_\alpha^{\sigma(eq)}(\mathbf{x},t)$ is the corresponding equilibrium particle distribution function; $\mathbf{e}_\alpha$ is the particle velocity in the αth direction, given as

$\mathbf{e}_\alpha = (0,0)$, for $\alpha = 0$,
$\mathbf{e}_\alpha = \left(\cos\theta_\alpha, \sin\theta_\alpha\right)\mathbf{c}$
with $\theta_\alpha = (\alpha-1)\pi/2$ for $\alpha = 1\text{-}4$,
$\mathbf{e}_\alpha = \sqrt{2}\left(\cos\theta_\alpha, \sin\theta_\alpha\right)\mathbf{c}$
with $\theta_\alpha = (\alpha-5)\pi/2 + \pi/4$ for $\alpha = 5\text{-}8$;

the superscript σ denotes different fluid components by specifying $\sigma = 1,2$, and τ^σ is the relaxation time of the σth fluid component depending on $v^\sigma = \left(\tau^\sigma - 1/2\right)\delta_t/3$. The density and velocity of each fluid component can be obtained by

$$\rho_\sigma = \sum_\alpha f_\alpha^\sigma \quad (2)$$

$$\mathbf{u}_\sigma = \frac{1}{\rho_\sigma}\sum_\alpha f_\alpha^\sigma \mathbf{e}_\alpha \quad (3)$$

The equilibrium particle distribution functions of each fluid component are of the forms as follows,

$$f_\alpha^{\sigma(eq)} = w_\alpha \rho_\sigma \left[1 + \frac{\mathbf{e}_\alpha \cdot \mathbf{u}_\sigma^{eq}}{c_s^2} + \frac{\left(\mathbf{e}_\alpha \cdot \mathbf{u}_\sigma^{eq}\right)^2}{2c_s^4} - \frac{\mathbf{u}_\sigma^{eq} \cdot \mathbf{u}_\sigma^{eq}}{2c_s^2}\right] \quad (4)$$

where $c_s = c/\sqrt{3}$ is defined as the lattice speed of sound, w_α is the weighting factor, with $w_\alpha = 4/9$ $(\alpha = 0)$, $w_\alpha = 1/9$ $(\alpha = 1-4)$ and $w_\alpha = 1/36$ $(\alpha = 5-8)$.

The fluid-fluid interaction and gravitational force are incorporated in Eq. (4) by modifying $\mathbf{u}_\sigma^{eq}$ as

$$\mathbf{u}_\sigma^{eq} = \mathbf{u}' + \frac{\tau^\sigma \mathbf{F}_\sigma}{\rho_\sigma} \quad (5)$$

where $\mathbf{F}_\sigma$ is the total force acting on the σth fluid component including the fluid-fluid interaction, and external force such as gravitational force, and $\mathbf{u}'$ is the common averaged velocity of all the fluid components in the absence of any additional forces, which is defined as (Shan and Doolen 1996)

$$\mathbf{u}' = \sum_{\sigma=1}^{2} \frac{\rho_\sigma \mathbf{u}_\sigma}{\tau^\sigma} \Bigg/ \sum_{\sigma=1}^{2} \frac{\rho_\sigma}{\tau^\sigma} \tag{6}$$

If only the interaction between the nearest neighbours and the next-nearest neighbours is taken into account, the fluid-fluid interaction is expressed as ((Shan and Chen 1993; Shan and Doolen 1995; Kang et al. 2002)

$$F_f^\sigma(\mathbf{x}) = -\psi_\sigma(\mathbf{x}) G_{\sigma\bar{\sigma}} \sum_{\mathbf{x}'} \sum_{\bar{\sigma}=1}^{2} \psi_{\bar{\sigma}}(\mathbf{x}') \mathbf{e}_\alpha \tag{7}$$

where $\psi_\sigma(\mathbf{x})$ is named "effective density" which is defined as a function of local particle density and assumed to be the local density ρ_σ in this study; $\mathbf{x}' = \mathbf{x} + \mathbf{e}_\alpha$ is the neighbour lattice of $\mathbf{x}$; and $G_{\sigma\bar{\sigma}}$ is the coefficient which controls the fluid-fluid interaction strength, given as

$G_{\sigma\bar{\sigma}} = G$ for $|\mathbf{e}_\alpha| = 1$,

$G_{\sigma\bar{\sigma}} = G/4$ for $|\mathbf{e}_\alpha| = \sqrt{2}$,

and $G_{\sigma\bar{\sigma}} = 0$ for otherwise.

Gravitational force can be simply introduced as

$$F_g^\sigma = \rho_\sigma g \tag{8}$$

where g is gravitational acceleration.

In the D2Q9 model, the pressure p of the whole fluid is given as (Shan et al. 1996).

$$p(\mathbf{x}) = c_s^2 \sum_\sigma \rho_\sigma(\mathbf{x}) + \frac{3}{2} G \psi_\sigma(\mathbf{x}) \psi_{\bar{\sigma}}(\mathbf{x}) \tag{9}$$

The viscosity of the fluid mixture is defined as $\nu = \left(\sum_\sigma x_\sigma \tau^\sigma - 1/2 \right) \Big/ 3$, where x_σ is the density fraction of the σth component.

3. Numerical Results and Discussion

It is well known that the flow behaviour of immiscible fluids in porous media is dictated by the competition of gravity, capillary force and viscous force. The gravity results in the interface of two immiscible fluids migration in the gravitational field. Viscous force and capillary force affect the movement of the interface. In addition, when the viscosities of the two fluids are dramatically different, the viscosity contrast will lead to the appearance of viscous finger. Dimensionless numbers are introduced to describe their influence. One is the capillary number, which gives the ratio of viscous force to capillary force. The general expression is given as $Ca = \nu\rho V/\gamma$, where ν is kinematic viscosity of the fluid; ρ is fluid density; V is velocity; and γ is surface tension. The ratio of gravity to capillary force is expressed by the Bond number, $Bo = \rho g L^2/\gamma$, where L is characteristic length (e.g. average pore radius). Another impact factor due to viscosity contrast is expressed by the viscosity ratio of displaced fluid to displacing fluid.

3.1. Simulation setup

Porous media is represented by a lattice system of 280x280 comprising 25 solid circles with a diameter of 20 lattice lengths in a staggered manner, as shown in Fig. 1. The porosity of porous media is $\phi = 0.9$. The black solid circles indicate the solid material in porous media, and the white regions serve as the path for the fluid to pass through. Line AB is located on the left hand side of the domain, with $OA = 10$.

Initially, at $x \geq A$, the research domain is filled with fluid 2 (displaced fluid)at rest, while, at $0 \leq x < A$, the region is occupied by fluid 1 (displacing fluid) with an initial velocity u_0 .The PDFs of fluid 1 and fluid 2 are specified with the equilibrium PDFs with zero velocity for fluid 2 and u_0 for fluid 1, respectively. Periodic boundary condition is applied in upper and lower boundaries. With

the simulation time marching, a constant velocity boundary scheme suggested by Zou (Zou and He 1997) is imposed on the inlet. Regarding the outlet, a zero derivative velocity condition is adopted. Bounce-back boundary scheme is adopted when the fluid encounters the solid materials. All variables are in lattice units, which can be related to physical units by dimensionless conversion.

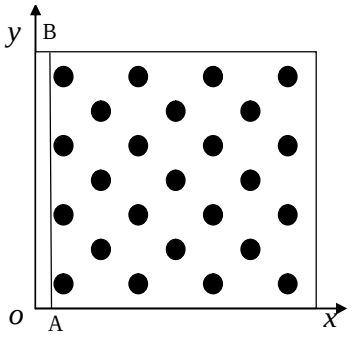

Fig. 1. Schematic diagram of simplified porous media

3.2. Evaluation of surface tension

Laplace's law $\Delta p = \gamma / R$ gives the relationship between the radii and pressure difference. In order to determine surface tension, a series of droplet tests with various radii is performed in a 100×100 lattice system. No external force, such as gravity, is applied. Periodic boundary condition is imposed on each boundary of the domain without taking wettability into account. Initially, different sizes of droplet are placed in the center of the lattice system, respectively, and then after a while, steady droplets of different radii can be obtained. The pressure inside and outside of the droplet is measured at the lattice that is far way from the interface, because the value of pressure may change sharply near the interface. The radius of the circle, on which the density of fluid 1 and fluid 2 are identical, is chosen as the radius of droplet at steady state. Regarding immiscible fluids with different viscosity ratios, four cases are studied ($M = 1,2,3,4$). After the pressure difference and droplet radii are measured, surface tension can be determined. The relationships of Δp and $1/R$ are plotted in Fig. 2. The solid discrete points represent lattice simulation results, and the line indicates linear regression results. The slopes of the line determine surface tension, which are tabulated in Table I, together with the intercept and the coefficient of determination R^2. As shown in Fig. 2, it is clear that the pressure difference inside and outside of the droplet is indeed proportional to the reciprocal of the droplet radium for all the cases.

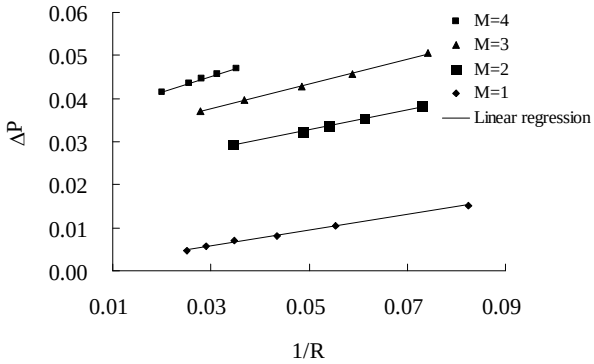

Fig. 2. Relationships between ΔP and $1/R$

Table 1: Surface tensions for fluids with different viscosity ratios

M	Surface tension	Intercept	R^2
1	0.1810	0.0004	0.9967
2	0.2296	0.0213	0.9959
3	0.2903	0.0289	0.9990
4	0.3666	0.0341	0.9982

3.3. Performance of numerical simulation

In this section, the effects of capillary number, Bond number, viscosity ratio on the immiscible fluid displacement process in simplified porous media are discussed. In this study, for simplicity, the density of fluid 1 and fluid 2 are unity, respectively, and the surface wettability is ignored.

3.3.1. Influence of capillary number

In order to investigate the effect of capillary number (*Ca*) on the fluid behaviour, several simulations with different capillary numbers are carried out by changing the initial velocity of the displacing fluid. Neither gravity nor viscosity ratio is considered. The interface between two immiscible fluids is defined as the region where the particle density of each

fluid component is identical. Three cases are studied with $Ca = 0.0088$, $Ca = 0.0265$ and $Ca = 0.0442$.

Figure 3 shows the interface positions with different capillary numbers. The grey circles represent the solid materials in porous media, and the white region and black region indicate the presence of displacing fluid and displaced fluid, respectively. It is simulated that at the early stage of displacement process, the interface moves evenly for all cases (shown on the left hand side of Fig. 3). However, in terms of Fig. 3(b)-Fig. 3(c), when *Ca* becomes relative large, significant isolated droplets of displaced fluid are formed either adhering to the solid materials or in the pore region.

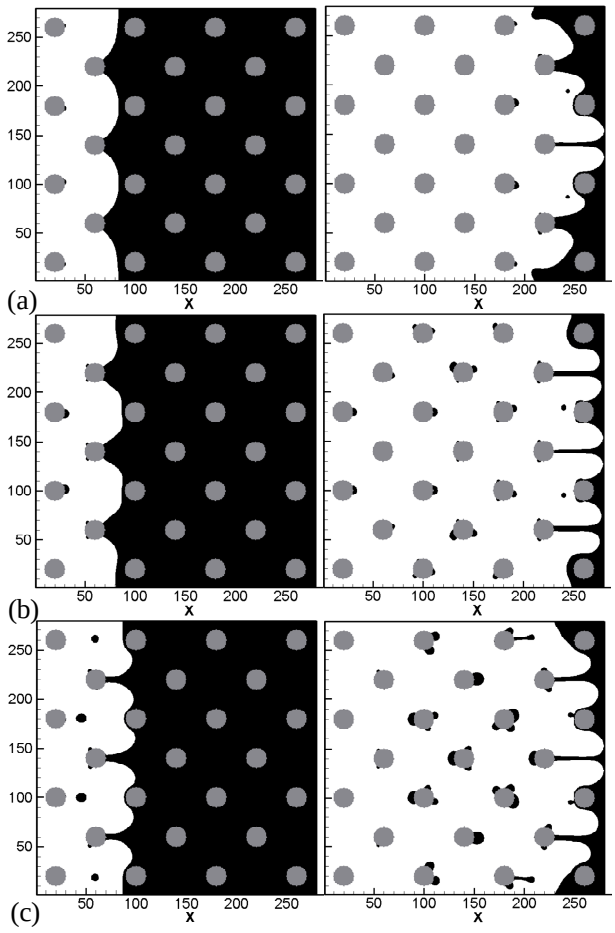

Fig. 3. The interface at early stage of the displacement (left hand side) and at final stage of the displacement (right hand side) for (a) *Ca* = 0.0088; (b) *Ca* = 0.0265; (c) *Ca* = 0.0442 .

In fact, even in the case of Fig. 3(a), small droplets are found in the region adhering to the solid materials. As shown on the right hand side of Fig. 3, when the interface fronts arrive at the outlet, fingers appear for all cases in a similar manner, but more isolated droplets of the displaced fluid are formed adhering to the solid material. Moreover, for $Ca = 0.0442$ (shown in Fig. 3(c)), the previously formed droplets in the pore region disappear.

The underlying mechanism behind the phenomenon is that relative small capillary number means the surface tension is dominant over the viscous force. Consequently, the surface tension provides a stabilizing effect at a short distance.

3.3.2. Influence of Bond number

It is well known that, if viscous fingering phenomenon happens, the finger pattern is symmetrical about the center line of research domain along x direction in the absence of gravity. However, when the gravity is taken into account, the finger pattern is no longer symmetrical. In order to study the effect of gravitational force on the finger pattern, the Bond number (*Bo*) is used to express the interplay between gravity and surface tension. Currently, viscosity ratio between the displaced fluid and the displacing fluid is set as $M = 3$, and the initial velocity of the displacing fluid is chosen as $u_0 = 0.03$. By changing gravitational acceleration g, which is applied along the negative direction of y axis, different Bond numbers can be obtained.

Figure 4 presents the interface positions at final stage of the displacement process with different Bond numbers. It is found out that for all cases, the interface front has a tendency to move downwards under the action of gravity. In addition, in the case of $Bo = 5.58$, the finger is the most obvious. For $Bo = 2.79$, the finger pattern is short and wide. In other two cases (shown in Fig. 4(c)-Fig. 4(d)), narrow and irregular fingers are formed, with some droplets of the displaced fluid either adhering to the solid materials or in the pore region.

Areal sweep efficiency Se, which is the ratio of the volume being swept by the displacing fluid to the total pore volume, is employed to indicate displacement efficiency.

The relationship between *Se* and *Bo* is shown in Fig. 5. When *Bo* is equal to 5.58, the highest sweep efficiency is found; when *Bo* is smaller than 5.58, *Se* decreases with *Bo*, and when *Bo* is bigger than 5.58, *Se* increases with *Bo*. Additionally, it is also found that, when the fingering phenomenon is the most significant, the areal sweep efficiency is the lowest.

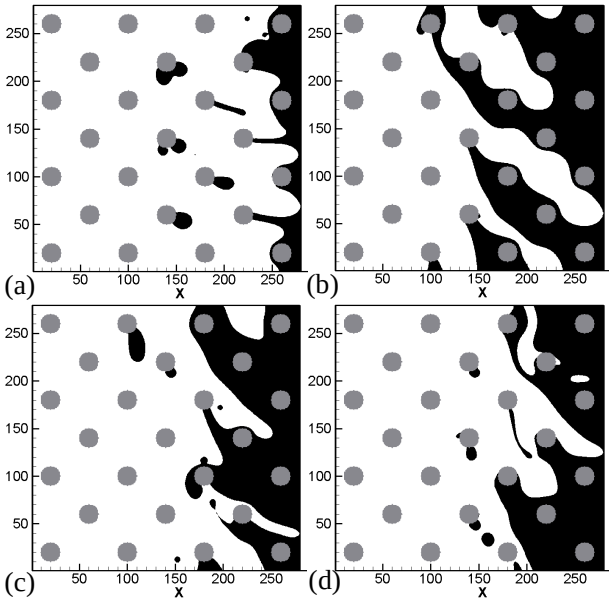

Fig. 4. Final finger patterns for (a) *Bo* = 2.79 ; (b) *Bo* = 5.58 ; (c) *Bo* = 8.37 ; (d) *Bo* = 11.16.

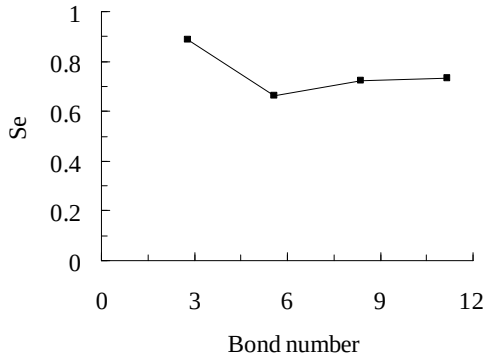

Fig. 5. Relationship between *Se* and Bond number.

3.3.3. Influence of viscosity ratio

The effect of viscosity ratio on the fluid behaviour has been analysed by performing a series of simulations with various viscosity ratios ($M = 1,2,3,4$) without consideration of gravity. The initial velocity of displacing fluid u_0 is fixed as 0.05 for each case.

When the interface reaches the outlet, the final interface patterns are compared, as shown in Fig. 6. It is modelled that for all cases, several fingers are formed at the late stage of the displacement. However, for $M \le 2$, some droplets of the displaced fluid are formed adhering to the solid materials. In addition, for $M \ge 3$, the finger patterns take on similar appearance. The increasing of viscosity ratio seems that it does not enhance further growth of the finger. One of the reasons may be that at the fixed velocity of the displacing fluid, the momentum introduced in the system is constant. However, more momentum is needed to displace higher viscous fluid. In addition, since the arrangement of solid materials is in a staggered manner, as a result the appearance of the solid obstacles in the front of the displacing fluid helps to suspend the occurrence of fingers.

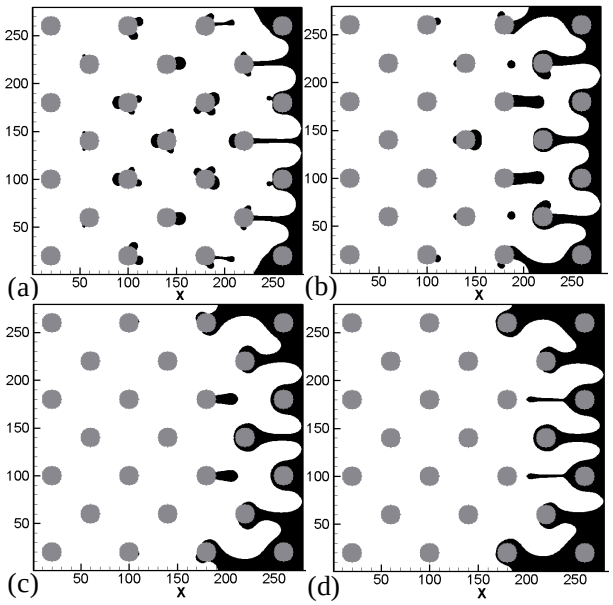

Fig. 6. Final finger patterns for (a) *M* = 1; (b) *M* = 2; (c) *M* = 3; (d) *M* = 4.

The relationship between areal sweep efficiency *Se* and viscosity ratio *M* is plotted in Fig. 7. It is found that areal sweep efficiency decreases with viscosity ratio, even if the final finger patterns are similar in the case of $M \ge 3$.

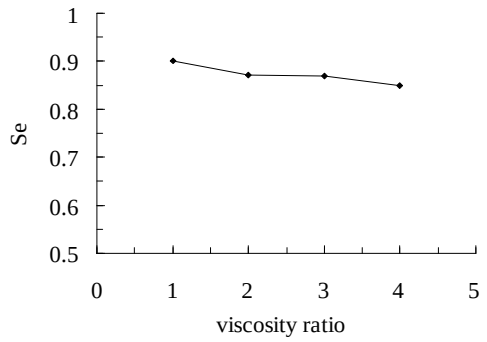

Fig. 7. Relationship between *Se* and viscosity ratio.

4. Conclusions

In this paper, the lattice Boltzmann method was adopted to study the effects of capillary number, Bond number, and viscosity ratio on the flow behaviour of immiscible fluid displacement process in simplified porous media.

It is found that the viscous fingering phenomenon is not obvious with the increasing of capillary number without consideration of gravity. However, more droplets of displaced fluid are formed adhering to the solid materials with capillary number. The viscous fingering phenomenon is obvious in the presence of gravity. Under the action of gravity, the finger front tends to move downwards in the direction of gravitational acceleration. The areal sweep efficiency is the lowest, when the viscous fingering is the most significant. In addition, it is modelled that the finger appearance is not enhanced dramatically in porous media which contains solid materials in staggered manner by increasing viscous ratio. Nevertheless, the areal sweep efficiency decreases with viscosity ratio.

In conclusion, the work suggests that the LBM is a reliable approach for the simulation of immiscible fluid displacement in porous media.

Acknowledgments

This work is supported by China Scholarship Council (CSC) for the first author's studying visit at University of Nottingham during the term from November 2007 to May 2009.

References

Grosfils, P., Boon, J. P., Chin, J., and Boek, E. S. 2004. Structural and dynamical characterization of Hele-Shaw viscous fingering, Philosophical Transactions of the Royal Society A: Mathematical, Physical and Engineering Sciences 362, 1723-1734.

Gunstensen, A. K., and Rothman, D. H. 1991. Lattice Boltzmann model of immiscible fluids, Phys. Rev. A 43, 4320-4327.

He, X., Chen, S., and Zhang, R. 1999. A lattice Boltzmann scheme for incompressible multiphase flow and its application in simulation of Rayleigh-Taylor instability, J. Comput. Phys. 152, 642-663.

Huang, H., Li, Z., Liu, S., and Lu, X.-y. 2008. Shan-and-Chen-type multiphase lattice Boltzmann study of viscous coupling effects for two-phase flow in porous media, International Journal for Numerical Methods in Fluids, 14.

Kang, Q., Zhang, D., and Chen, S. 2002. Displacement of a two-dimensional immiscible droplet in a channel, Physics of Fluids 14, 3203-3214.

Luo, L. 1998. Unified theory of lattice Boltzmann models for nonideal gases, Phys. Rev. Lett. 81, 1618-1621.

Luo, L. 2000. Theory of the lattice Boltzmann method: Lattice Boltzmann models for nonideal gases, Phys. Rev. E 62, 4982-4996.

Shan, X., and Chen, H. 1993. Lattice Boltzmann model for simulating flows with multiple phases and components, Phys. Rev. E 47, 1815-1819.

Shan, X., and Doolen, G. 1995. Multicomponent lattice-Boltzmann model with interparticle interaction, Journal of Statistical Physics 81, 379-393.

Shan, X., and Doolen, G. 1996. Diffusion in a multicomponent lattice Boltzmann equation model, Phys. Rev. E 54, 3614-3620.

Swift, M. R., Orlandini, E., W. R, O., and Yeomans, J. M. 1996. Lattice Boltzmann simulations of liquid-gas and binary fluid systems, Phys. Rev. E 54, 5041-5052.

Swift, M. R., W. R, O., and Yeomans, J. M. 1995. Lattice Boltzmann Simulation of Nonideal Fluids, Phys. Rev. Lett. 75, 830-833.

van Kats, F. M., and Egberts, P. J. P. 1999. Simulation of three-phase displacement mechanisms using a 2D lattice-Boltzmann model, Transport in Porous Media 37, 55-68.

Yiotis, A. G., Psihogios, J., Kainourgiakis, M. E., Papaioannou, A., and Stubos, A. K. 2007. A lattice Boltzmann study of viscous coupling effects in immiscible two-phase flow in porous media, Colloids and Surfaces A: Physicochemical and Engineering Aspects 300, 35-49.

Zou, Q., and He, X. 1997. On pressure and velocity boundary conditions for the lattice Boltzmann BGK model, Phys. Fluids 9, 1591-1598.